# Assessment of Microelastic Properties of Bone Using Scanning Acoustic Microscopy: A Face-to-Face Comparison with Nanoindentation

Fabienne Rupin[1,2], Amena Saïed[1,2*], Davy Dalmas[3], Françoise Peyrin[4], Sylvain Haupert[1,2], Kay Raum[5], Etienne Barthel[3], Georges Boivin[6], and Pascal Laugier[1,2]

[1]*Université Pierre et Marie Curie-Paris6, Laboratoire d'Imagerie Paramétrique, Paris F-75005, France*
[2]*CNRS, LIP, Paris F-75006, France*
[3]*Unité Mixte CNRS/Saint-Gobain "Surface du Verre et Interface" UMR 125, Saint-Gobain Recherche, Aubervilliers F-93303, France*
[4]*ESRF/CREATIS, Grenoble 38043, France*
[5]*Q-BAM Group, Dept. of Orthopedics, Martin Luther University of Halle-Wittenberg, 06097 Halle, Germany*
[6]*INSERM Unité 831, Faculté de Médecine Laennec, Université de Lyon, Lyon 69372, France*

Received November 19, 2008; accepted February 25, 2009; published online July 21, 2009

The current work aimed at comparing, on site-matched cortical bone tissue, the micron-level elastic modulus $E_a$ derived from 200 MHz-scanning acoustic microscopy (SAM) acoustic impedance ($Z$) combined with bone mineral density (assessed by synchrotron radiation microcomputed tomography, SR-μCT) to nanoindentation modulus $E_n$. A good correlation was observed between $E_n$ and $Z$ ($R^2 = 0.67$, $p < 0.0001$, root mean square error RMSE = 1.9 GPa). The acoustical elastic modulus $E_a$ derived from $Z$ showed higher values of $E$ compared to nanoindentation moduli. We assumed that the discrepancy between $E_a$ and $E_n$ values may likely be due to the fixed assumed value of Poisson's ratio while values comprised between 0.15 and 0.45 have been reported in the literature. Despite these differences, a highly significant correlation between $E_a$ and $E_n$ was found ($R^2 = 0.66$, $p < 0.001$, RMSE = 1.8 GPa) suggesting that SAM can reliably be used as a modality to quantitatively map the local variations of tissue-level bone elasticity. 

**DOI:** 10.1143/JJAP.48.07GK01

## 1. Introduction

Bone is one of the most challenging complex biocomposite material that has become the focus of extensive studies in light of population aging and associated bone pathologies.[1,2] Bone is built primarily of nanoscale sized collagen fibrils and apatite mineral crystals that are arranged in several hierarchical levels. This multiple level of hierarchical organization enables bone to properly adapt to its functional environment.[3,4] The mechanical properties of bone are, therefore, dependent upon structural, amount and compositional properties of tissue constituents and change with changes in scale, anatomical location and orientation.[5] Mature human cortical bone is mainly composed of tubelike structures called osteons embedded in a matrix of interstitial tissue made of partially remodelled osteons or primary bone tissue.[6,7] Each osteon (200–250 μm in diameter) is formed of concentric lamellae (3–5 μm thick) surrounding a central blood vessel.[8] Within a lamella the mineralised collagen fibrils run helically around the central canal with regular changes in their orientation.[9] Given the complexity of the structural organization of bone, the knowledge of intrinsic micromechanical properties of cortical tissue is of utmost importance for many research and clinical problems. In particular, it contributes to provide insights into how collagen network and mineralization correlate to the intrinsic mechanical properties of normal tissue and elucidate mechanisms involved in bone alteration due to various metabolically diseased and pharmacologically treated conditions. Also, it may provide inputs for numerical computational models to predict mechanical behavior of whole bone and implant systems. Nanoindentation is a mechanical micro-probe-techniques widely used to investigate finely structured materials and is currently the only established method commonly used for a direct measurement of intrinsic mechanical properties of bone at the lamellar level.[10–12] Many studies have shown that these mechanical properties vary within bone (osteonal and interstitial tissues),[7,11,13] between species[3] and individuals,[14] with bone anatomical location[15,16] and direction of testing.[17–19] However, the influence of spatial distribution of tissue constituent properties on the spatial variations in mechanical properties at the micron level has received less important consideration. Few quantitative studies reported on how tissue mineralization may be related to nanoindentation elastic modulus.[20–22]

Despite improvements in the instrument accuracy, nanoindentation has limited capabilities for accurate mapping of the spatial variation in bone heterogeneous mechanical properties. First, measurements are constrained to discrete levels, thus jeopardizing a comprehensive evaluation of the non-uniform microstructure of bone. Secondly, nanoindentation is inherently destructive leaving a permanent plastic deformation created by the indenter tip. Subsequently scanning acoustic microscopy (SAM) is an attractive non-contact imaging modality able to map, over a large surface, the spatial distribution of micro-elastic properties. Using a set of calibration materials, the signal reflectivity from the sample surface can be converted into an acoustical impedance value which is well modeled as the square root of the product of the local mass density and local stiffness coefficient in the test direction. When the local density (or mineralization) is experimentally ascertained, such as with micro-computed tomography (μ-CT), for example, the stiffness coefficient can be computed and subsequently, tissue-level elastic modulus can be derived from acoustical impedance measurements. As an extension of previous SAM-based acoustic impedance studies reported by our group.[23–26] The current work aimed at validating acoustic microscopy as a modality to map elastic modulus at the tissue-level. Toward this goal a face-to-face comparison was conducted between SAM and nanoindentation estimates of elastic modulus on site-matched regions of human femoral cortical bone.

*E-mail address: saied@lip.bhdc.jussieu.fr

 

## 2. Materials and Methods

### 2.1 Bone samples

Two Cortical bone transverse cross-sections (10 mm in thickness) were extracted from the mid-diaphysis of the right femurs of two women cadavers of 78 and 85 year old. Ethical approval for collection of samples was granted by the Human Ethics Committee of the Centre des dons du corps at the University René Descartes (Paris, France). The tissue donors or their legal guardians provided informed written consent to give their tissue for investigation, in accord with legal clauses stated in the French Code of Public Health.

Each cross-section was cut in four specimens corresponding to the four anatomical quadrants (posterior, anterior, medial and lateral). The specimens ($n = 8$) were fixed and dehydrated in 70% ethanol and embedded in poly-(methyl methacrylate) (PMMA). The face (cross-section oriented perpendicular to the femur axis) of each block was carefully grinded then polished to obtain smooth surface on microcloths with successively finer grades of alumina powder, the finest being 0.05 μm grit. Finally, the specimens were ultrasonically cleaned in de-ionized water to remove surface debris.[12)]

### 2.2 Scanning acoustic microscopy

#### 2.2.1 Data acquisition procedure

The principles of scanning acoustic microscopy has widely been described in previous work reported by our group.[23,24,26)] Here, the samples were explored using a SAM 200 developed in our laboratory. The system operated with a 200 MHz focusing transducer having a 490 μm focal length and a 60° full aperture angle (Fraunhofer Institute for Biomedical Engineering, St. Ingbert, Germany). The nominal lateral resolution was approximately 8 μm in water at 25 °C. The transducer was excited by a 200 MHz pulser receiver (Panametrics 5900 PR). Before data acquisition, the bone sample to be explored was completely immersed in a temperature-controlled (25 °C) distilled water bath and its polished surface was adjusted to be positioned at the transducer focus and perfectly perpendicular to the ultrasound beam axis. *C*-scan images were formed by displacing the transducer over the specimen surface with a 5 μm translational step using two stepping motors providing a 0.5 μm positional resolution (Micro-Controle Spectra-Physics Newport M-ILS200PP). At each scan point, the reflected echo signal was acquired under fixed electronic settings at 1 GHz sampling rate using a 8-bit-digitizer (Agilent Acquiris DP240). The pulser-receiver settings, transducer displacement and data acquisition were controlled by a labview based custom developed software.

#### 2.2.2 Estimation of acoustic impedance

Calibrated images of acoustic impedance ($Z$) have been obtained using a Matlab based software.[23–26)] Briefly, each pixel of the reflected amplitude image of bone (map of the maximum amplitude of the envelope of the reflected voltage) was converted into a local $Z$ value by means of a calibration curve correlating the local reflected signal amplitude of a set of isotropic homogeneous materials (PMMA, polycarbonate, aluminum, and titanium) with their corresponding pre-determined acoustic impedance.[27,28)] These calibration materials were systematically measured before each bone sample evaluation under the same electronic settings and experimental conditions. The assessment of the distribution of $Z$ values of bone tissue was made on impedance maps by separating bone from surrounding PMMA using a previously reported thresholding method.[23,24,29)]

### 2.3 Nanoindentation

After SAM acquisition, nanoindentation tests were performed using a nanoindenter XP system (MTS Nano Instruments) with a Berkovich diamond tip. Measurements were performed at room temperature under dry conditions on the bone regions explored by SAM. The elastic modulus was determined using the common method and equations developed by Oliver and Pharr[30,31)] that has been used to characterize bone tissue in nearly all literature studies. The Young's Modulus is calculated under the assumption that bone tissue is elastically isotropic and homogeneous as follows:

$$\frac{1}{E_r} = \frac{(1 - \upsilon_s^2)}{E_n} + \frac{(1 - \upsilon_i{}^2)}{E_i}, \quad (1)$$

where $E_r$ is the effective indentation modulus, $\upsilon$ is Poisson's ratio (s and i referring to sample and indenter tip material respectively). $E_n$ is the elastic modulus of the specimen. $\upsilon_s$ was set to 0.3 and the elastic properties of the diamond indenter tip were $\upsilon_i = 0.07$ and $E_i = 1141$ GPa.

The continuous stiffness measurement (CSM) technique was used, which records stiffness data along with load and displacement data and, therefore, leads to a direct and continuous measure of dynamic contact stiffness elastic modulus as a function of the depth of the indentation.[30,32)] This method has been shown to be somewhat insensitive to thermal drift and allows an accurate observation of small volume deformation.[33)] CSM was performed using a 5 nm magnitude oscillation with a frequency of 45 Hz. A standard calibration silica material was used to calibrate the tip shape function and check the analysis procedures.

The strain rate was constant during the experiments ($0.05\ s^{-1}$) and the surface penetration depth was fixed to 2 μm in order to probe similar near surface volume than with SAM and obtain residual indents observable with SAM resolution (approximately 8–10 μm). When the tip was at the maximum penetration depth, the load was maintained constant during 150 s.

Sixty nanoindentation tests were performed at each bone quadrant (along the radial direction from the endosteal to the periosteal cortex). Three target areas including osteons and interstitial tissue were selected in the endoste, middle, and perioste. At each site, 20 measurements in 2 line scans (10 indents each with 30-μm-spacing in both directions) were made. Additionally, in order to further identify each subcortical indented region, four indent marks, 5-μm-deep were made (each at 100 μm distance from the region) to encompass the twenty indents. After nanoindentation tests were completed, the indented region of interest of each quadrant was imaged again with SAM to visualize the location of residual indents and match positions of which $Z$ and $E_n$ were measured. All indents falling into PMMA area or in the boundary between PMMA and bone were not taken

into account for further analysis. Some indents were also excluded since the nanoindentation mark and curve were not satisfying. The analysis was made on 329 nanoindentation data points.

### 2.4 Synchrotron microtomography acquisition

After SAM and nanoindentation measurements, the samples were imaged using synchrotron radiation microtomography (SR-μCT) at the European Synchrotron Radiation Facility (ESRF, Grenoble, France) in order to determine the three-dimensional (3D) distribution of the degree of mineralization of bone (DMB). 3D images of bone samples were acquired on Beamline ID19 with a 5.1 μm pixel size allowing a spatial resolution of 10 μm (comparable to that of SAM and nanoindentation) and a field of view of $10 \times 10\,\mathrm{mm}^2$. The energy was set to 28 keV and 1800 radiographic images under different angles of view were recorded. The tomographic reconstruction of 3D images and the estimation of mean DMB are well described in ref. 34.

### 2.5 Multi-modality images fusion

The SAM images before and after nanoindentation, and DMB maps of each bone sample were digitally matched using the image registration tools of Matlab (Mathworks) and a custom developed image fusion and analysis Matlab-based software.[23,35] By matching the positions at which $Z$, $E_n$, and DMB were measured (Fig. 1), the procedure allows a direct comparison of $Z$, $E_a$, and $E_n$ in the same region of interest (ROI). $Z$ and DMB values and subsequently $E_a$ were obtained by averaging value in a ROI of $3 \times 3$ pixels$^2$ ($15 \times 15\,\mu\mathrm{m}^2$) covering the entire surface of the residual contact area left by the indents.

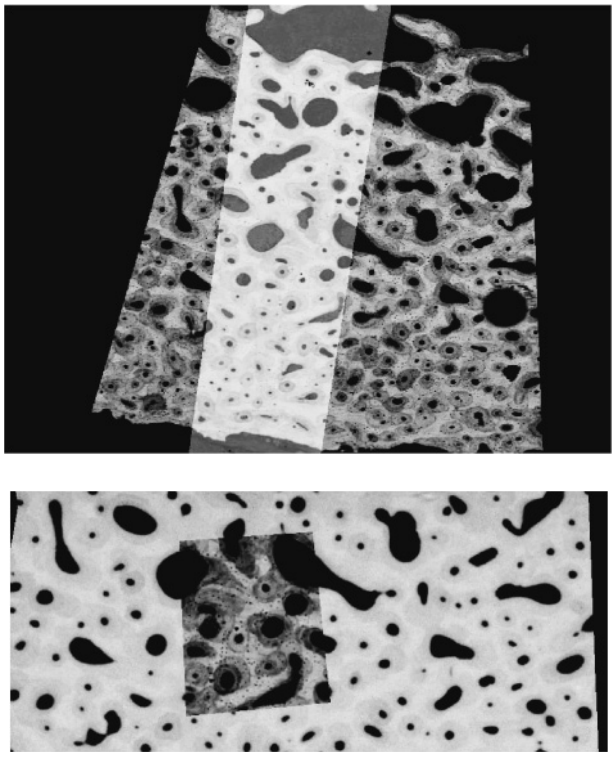

**Fig. 1.** SAM image before nanoindentation fused with SAM image after nanoindentation (up) and SR-μCT image fused with SAM image after nanoindentation (down).

### 2.6 Determination of acoustic Young's modulus $E_a$

For transverse isotropic material, the anisotropic elastic coefficient in the probing direction can be expressed as a combination of $Z$ and bone mass density $\rho$:

$$C_{ii} = \frac{Z_i^2}{\rho}. \tag{2}$$

Since acoustic wave propagates in the bulk mode, $E_a$ and $C_{33}$ are linked as follows:

$$E_a = \frac{(1+\upsilon_{12})(1-\upsilon_{12}-2\upsilon_{13}\upsilon_{31})}{(1-\upsilon_{12}{}^2)} C_{33}, \tag{3}$$

where $x_3$ is the longitudinal direction and $(x_1, x_2)$ is the cross-section plane. $\upsilon_{ij}$ is the Poisson's ratio in the corresponding plane assumed to be equal to 0.3. In this condition, the relation between $E_3$ and $C_{33}$ becomes

$$E_a = 0.7429 \cdot C_{33}. \tag{4}$$

In eq. (2), bone mass density $\rho$ was derived from DMB measurements using a rule of mixture model relating tissue mass density to the mass density and volume fraction of tissue bone components (collagen, mineral, and water replaced here by PMMA).[24,36]

Each pixel of site matched $Z$ and DMB maps will be converted in a $E_a$ pixel as follows:

$$E_a = \frac{0.7429 \cdot Z^2}{(1.25 + 0.64 \cdot \mathrm{DMB} - 0.02 \cdot \mathrm{DMB}^2)}. \tag{5}$$

### 2.7 Statistics

Regression analysis and Pearson's regression coefficient were used to describe the relationship between $Z$, $E_a$, and $E_n$. Values of $p < 0.05$ were considered statistically significant. The statistical analysis was performed using the NCSS software, version 2000, NCSS, Utah, USA.

## 3. Results

### 3.1 Reproducibility and accuracy

SAM reproducibility was determined by the measurements of five bone samples two times. The average relative error of the estimated mean impedance given by the root mean square average of the five relative standard deviations was 1.7%. SR-μCT relative error of DMB was estimated in previous work[34] and has been reported to be 0.26%. Because nanoindentation tests leave plastic deformation preventing repetitive measurement at the same bone location, nanoindentation reproducibility was estimated by measuring, at 3 different days, 50 times at 3 different locations, the Young's modulus of silica. The estimated relative error was 2%.

### 3.2 Elastic moduli of calibrated materials

Prior to bone evaluation, nanoindentation and SAM measurements were performed on homogeneous calibrated materials (aluminium, PMMA, and polycarbonate) of known Poisson's ratio and density. Acoustic elastic moduli were derived from $Z$ measurements and compared to $E$ obtained by nanoindentation. The results are presented in Table I. The acoustic and nanoindentation moduli yielded a difference of less than 1.3%.

**Table I.** Comparison of the Young's modulus of homogeneous material determined by nanoindentation and acoustic microscopy. Each material had been measured 10 times. The mass density and the Poisson's ratio were obtained from the literature.

| Material | $Z$ (Mrayl) | $E_n$ (GPa) | $\rho$ (g/cm$^3$) | $v$ | $E_a$ (GPa) |
|---|---|---|---|---|---|
| Al | $17.1 \pm 1.1$ | $69.8 \pm 2.5$ | 2.69 | 0.345 | $69.2 \pm 5.4$ |
| PMMA | $3.3 \pm 0.1$ | $4.4 \pm 0.1$ | 1.18 | 0.39 | $4.5 \pm 0.2$ |
| PC | $2.7 \pm 0.1$ | $3.2 \pm 0.1$ | 1.2 | 0.38 | $3.4 \pm 0.2$ |

### 3.3 Parameters of bone

Due to experimental issues, one quadrant was excluded from the analysis.

For each sample, we calculated the mean value of $Z$, DMB, $E_n$, and $E_a$ averaged over all measurement points. Mean values of the four estimated parameters were also averaged over the seven samples.

$Z$ value of bone obtained from all the measurement points ranged between 5 and 13 Mrayl (mean $= 9.1 \pm 1.7$ Mrayl). $E_n$ value obtained from all the indentation points ranged between 11 and 27 GPa, mean $= 19.5 \pm 3$ GPa. Bone densities derived from DMB was found to be $1.84 \pm 0.04$ g/cm$^3$.

$E_a$ measured at all bone locations varied between 10 and 65 GPa (mean $= 35 \pm 11$ GPa). The values of acoustic elastic modulus was substantially greater to nanoindentation modulus was obtained ($E_a$ being nearly two times higher than $E_n$).

All variables were significantly correlated, however, a higher correlation was found between $Z$ and DMB ($R^2 = 0.53$, $p < 0.001$) than between $E_n$ and DMB ($R^2 = 0.38$). In addition, $Z$ was best predicted with a multiple regression model including both the density and the modulus $E_n$ ($R^2 = 0.75$, $p < 0.0001$). These results reflect the influence of density on the acoustical impedance as indicated by eq. (2). For all the bone samples, a good correlation was observed between $E_n$ and $Z$ ($r = 0.81$, $R^2 = 0.67$, $p < 0.0001$, RMSE $= 1.9$ GPa) as illustrated in Fig. 2. When $E_n$ was confronted to its acoustic equivalent, a highly significant linear correlation between $E_a$ and $E_n$ could be observed as well (Fig. 3). The correlation coefficient was similar to the one between $Z$ and $E_n$ ($r = 0.81$, $R^2 = 0.66$, $p < 0.0001$, RMSE $= 1.8$ GPa).

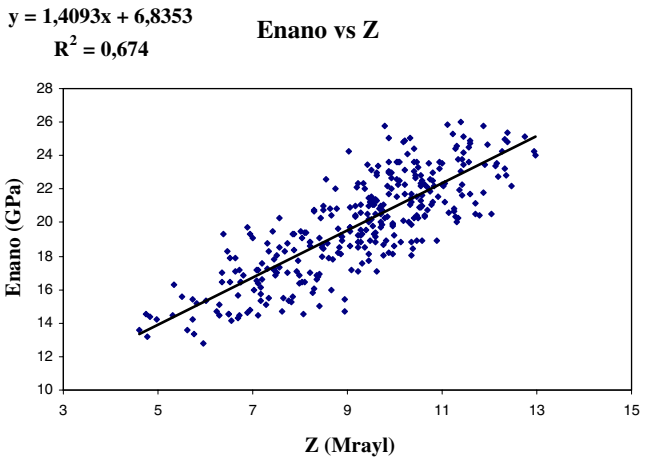


**Fig. 2.** (Color online) Correlation curve between $Z$ measured by acoustic microscopy and $E_n$ derived from nanoindentation.

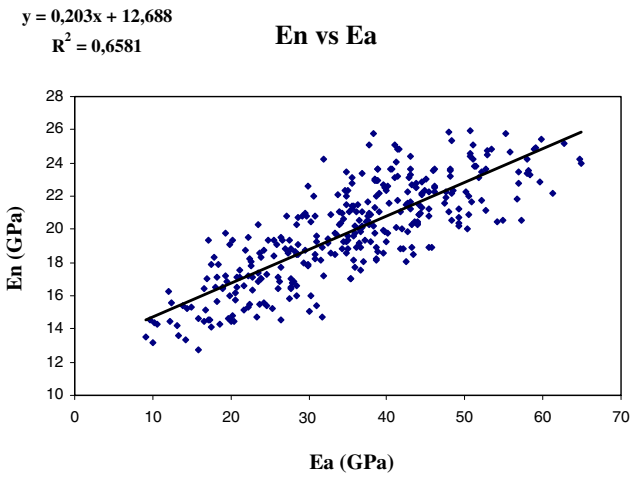


**Fig. 3.** (Color online) Correlation curve between $E_a$ measured by acoustic microscopy and $E_n$ derived from nanoindentation.

## 4. Discussion and Conclusions

The present study is the first to describe, on the basis of site-matched cortical bone tissue, a face to face comparison between nanoindentation modulus and acoustically derived elastic modulus. The acoustically derived modulus is computed from 200 MHz-scanning acoustic microscope-based impedance combined with bone density determined by SR-μCT.

The nanoindentation elastic modulus of cross-sections taken from femurs of two donor were consistent with reported values by other groups on femur.[7,11,22,24,37–39] Mean value of acoustic impedance are within the range of values previously reported by other investigators on human femoral cortical bone at 100 and 400 MHz (20 and 2.5 μm lateral resolutions, respectively).[27,40]

Independently of bone tissue location within the cortex, young modulus generated from acoustic impedance was substantially greater than nanoindentation modulus, being nearly 2 times higher than $E_n$. The correlation coefficient between the two moduli was as high as that found between $Z$ and $E_n$. Our findings do not corroborate two conflicting earlier studies comparing nanoindentation modulus to elastic modulus derived from 50 MHz acoustic microscopy-based on bulk velocity measurement. Turner *et al.*[41] reported opposite result: nanoindentation modulus was 14% greater than modulus measured by acoustic microscopy, while Hengsberger *et al.*[13] have found that SAM elastic modulus was significantly higher than nanoindentation modulus and was within the range of our values, but the two moduli were not correlated. It is important to note that our validation study performed on homogeneous materials of known density and Poisson ratio, demonstrated that ultrasonically and mechanically determined Young's moduli were similar. This latter result corroborates previous reported findings[42] and supports the accuracy of our measuring protocol. Furthermore, the findings suggests that the discrepancy between $E_a$ and $E_n$ observed in heterogeneous and aniso-

tropic bone tissue may mostly be attributed to the *a priori* value of $\upsilon_b = 0.3$ assigned to the Poisson's ratio. As the spatial variation in microscale value of Poisson's ratio is not known in bone tissue and was not concurrently measured on our samples, this chosen value of $\upsilon$ corresponds to an average of a wide range of reported values extending from 0.15 to 0.45, measured at various scales using multiple techniques.[5,43,44] This wide range of values of Poisson's ratio may lead to $E_a$ values within 12 and 45 GPa and $E_n$ between 17 and 21 GPa, indicating that the calculated nanoindentation modulus is fairly insensitive to the variation in $\upsilon$ value. For example, varying $\upsilon$ by $\pm 10\%$ results in only $\pm 2\%$ variation in $E_n$ while it affects dramatically elastic modulus derived from SAM which varies by as much as Poisson's ratio ($\pm 10\%$). Therefore, unknown local variations in the Poisson's ratio are likely to be strongly reflected in $E_a$ but to a much lesser extent in $E_n$, which supports the idea that most of the unexplained variability between $E_n$ and $E_a$ is related to these uncontrolled variations in Poisson's ratio. The determination of the Poisson's ratio at the tissue scale becomes hence, a major issue for the accurate assessment of the elastic modulus using acoustic microscopy. Further investigations will be required to test the effect of Poisson's ratio on combined mechanical and ultrasonic assessments of elastic modulus.

Other experimental and theoretical issues need to be considered. Even though ultrasound and mechanical measurements were made at the same locations of the bone specimens, additional experimental and theoretical factors may explain the lacking (almost 30%) correlation between acoustic parameters ($Z$ or $E_a$) and nanoindentation modulus such as (i) difference in near surface probed volume; SAM penetration depth is estimated to be equivalent to one wavelength i.e. 20 µm in cortical bone at 200 MHz, while nanoindentation penetration depth is generally considered to be three to five times the fixed penetration depth of the indenter tip (here 2 µm), i.e., 6 to 10 µm; (ii) measurements are taken under different experimental conditions (dry and quasi-static measurements for nanoindentation, dynamic measurements in immersion with SAM); this may affect the visco-elastic response of the specimens[45] and ultimately the measured moduli; (iii) usual hypotheses underlying the theoretical framework used to derive $E_n$ and $E_a$ from mechanical or ultrasonic testing include isotropy, homogeneity and fixed value of Poisson's ratio. Further work is required to elucidate the impact of these hypotheses on the outcome of the calculation of the acoustic and nanoindentation moduli.

With regards to the influence of mineral density on tissue elasticity, our results indicated a fairly moderate correlation between nanoindentation modulus and mineralization ($R^2 = 0.38$) but a stronger influence of mineralization on the acoustical impedance ($R^2 = 0.53$). The few existing studies reported controversial conclusions. Hoc *et al.*[22] reported a high correlation coefficient ($R^2 = 0.75$) between local nanoindentation modulus and mineral content of mature bovine cortical bone. Gupta *et al.*[20] observed a significantly high positive correlation between nanoindentation stiffness and calcium content of human compact bone. Hengsberger *et al.*[13] have shown that nanoindentation was weakly correlated to mineralization and the acoustic elastic modulus was better related to DMB of human compact bone. Of note is that none of the previous studies have presented such a stringent protocol as in our study. The strengths of our study rely (i) on preliminary tests on calibrated materials: such tests document the accuracy of our results, and (ii) on a strict site-matching control based on automatic image processing ensuring that exactly the same regions were assessed mechanically and ultrasonically. Such a protocol designed to minimize measurements errors suggest that the unexplained variance between modulus and DMB has to be found in other parameters that were not controlled, such as ultrastructural features including collagen fibers orientation and size and orientations of hydroxyapatite crystals.

The higher correlation between mineralization and acoustic impedance compared to the relationship between $E_n$ and mineralization was expected as a direct result from eq. (2) indicating that the acoustical impedance is directly proportional to the square root of the density. In the present study, the acoustic determination of elastic modulus relied on the evaluation of bone density derived from site-matched DMB measurements. An appropriate and accurate measurement or model of the density is required to correct the acoustical impedance data and extract an accurate value of the stiffness and of the modulus. Nevertheless, in addition to the good correlation between $E_a$ and $E_n$, we have found that $Z$ was able to determine $E_n$ within a 10% RMSE suggesting that SAM-based acoustic impedance is a valuable tool and may potentially be used to provide data on the spatial distribution of micro-elastic bone properties.

In summary, quantitative SAM displays properties of bone in high resolution 2D images and has the advantage to measure data on the spatial distribution of micro-elastic bone properties (stiffness), whereas nanoindentation provides measurements at discrete levels. These micromechanical properties are not fully determined by amount of the mineral alone but are also influenced by ultrastructural factors such as collagen fiber orientation, characteristics of mineral, and arrangements of these materials.


1) F. Padilla, Q. Grimal, and P. Laugier: Jpn. J. Appl. Phys. **47** (2008) 4220.
2) F. Padilla, E. Bossy, and P. Laugier: Jpn. J. Appl. Phys. **45** (2006) 6496.
3) J. D. Currey: J. Biomech. **36** (2003) 1487.
4) D. B. Burr: Bone **31** (2002) 8.
5) J. Currey: *Bones:Structure and Mechanics* (Princeton University Press, Princeton, NJ, 2002).
6) D. B. Burr, M. B. Schaffler, and R. G. Frederickson: J. Biomech. **21** (1988) 939.
7) J. Y. Rho, P. Zioupos, J. D. Currey, and G. M. Pharr: Bone **25** (1999) 295.
8) P. Fratzl, H. S. Gupta, E. P. Paschalis, and P. Roschger: J. Mater. Chem. **14** (2004) 2115.
9) M. M. Giraud-Guille, L. Besseau, and R. Martin: J. Biomech. **36** (2003) 1571.
10) C. E. Hoffler, K. E. Moore, K. Kozloff, P. K. Zysset, M. B. Brown, and S. A. Goldstein: Bone **26** (2000) 603.
11) J. Y. Rho, P. Zioupos, J. D. Currey, and G. M. Pharr: J. Biomech. **35** (2002) 189.
12) P. K. Zysset, X. E. Guo, C. E. Hoffler, K. E. Moore, and S. A. Goldstein: J. Biomech. **32** (1999) 1005.
13) S. Hengsberger, G. Boivin, and P. K. Zysset: JSME **45** (2002) 936.
14) P. K. Zysset, R. W. Goulet, and S. J. Hollister: J. Biomech. Eng. **120**

(1998) 640.
15) J. Y. Rho, J. D. Currey, P. Zioupos, and G. M. Pharr: J. Exp. Biol. **204** (2001) 1775.
16) S. Hengsberger, P. Ammann, B. Legros, R. Rizzoli, and P. Zysset: Bone **36** (2005) 134.
17) J. Y. Rho, Y. T. Tsui, and G. M. Pharr: Biomaterials **18** (1997) 1325.
18) J. Y. Rho, M. E. Roy, Y. T. Tsui, and G. M. Pharr: J. Biomed. Mater. Res. **45** (1999) 48.
19) M. E. Roy, J. Y. Rho, Y. T. Tsui, N. D. Evans, and G. M. Pharr: J. Biomed. Mater. Res. **44** (1999) 191.
20) H. S. Gupta, U. Stachewicz, W. Wagermaier, P. Roschger, H. D. Wagner, and P. Fratzl: J. Mater. Res. **21** (2006) 1913.
21) T. Hofmann, F. Heyroth, H. Meinhard, W. Franzel, and K. Raum: J. Biomech. **39** (2006) 2282.
22) T. Hoc, L. Henry, M. Verdier, D. Aubry, L. Sedel, and A. Meunier: Bone **38** (2006) 466.
23) K. Raum, I. Leguerney, F. Chandelier, M. Talmant, A. Saied, F. Peyrin, and P. Laugier: Phys. Med. Biol. **51** (2006) 733.
24) K. Raum, R. O. Cleveland, F. Peyrin, and P. Laugier: Phys. Med. Biol. **51** (2006) 747.
25) K. Raum, T. Hofmann, I. Leguerney, A. Saied, F. Peyrin, L. Vico, and P. Laugier: Bone **41** (2007) 1017.
26) A. Saied, K. Raum, I. Leguerney, and P. Laugier: Bone **43** (2008) 187.
27) K. Raum, J. Reisshauer, and J. Brandt: J. Biomed. Mater. Res., Part A **71A** (2004) 430.
28) S. Bumrerraj and J. L. Katz: Ann. Biomed. Eng. **29** (2001) 1034.
29) K. Raum, K. V. Jenderka, A. Klemenz, and J. Brandt: IEEE Ultrasonics Symp. Proc., 2002, Vols. 1 and 2, p. 1345.
30) W. C. Oliver and G. M. Pharr: J. Mater. Res. **7** (1992) 1564.
31) W. C. Oliver and G. M. Pharr: J. Mater. Res. **19** (2004) 3.
32) X. Wang, M. R. Allen, D. B. Burr, E. J. Lavernia, B. Jeremic, and D. R. Fyhrie: Bone **43** (2008) 775.
33) X. Li and B. Bhushan: Mater. Charact. **48** (2002) 11.
34) S. Nuzzo, F. Peyrin, P. Cloetens, J. Baruchel, and G. Boivin: Med. Phys. **29** (2002) 2672.
35) K. Raum, I. Leguerney, F. Chandelier, E. Bossy, M. Talmant, A. Saied, F. Peyrin, and P. Laugier: Ultrasound Med. Biol. **31** (2005) 1225.
36) T. Hofman, K. Raum, I. Leguerney, A. Saied, F. Peyrin, L. Vico, and P. Laugier: Ultrasonics **44** (2006) E1307.
37) H. Gupta, U. Stachewicz, and W. Wagermaier: J. Mater. Res. **21** (2008) 1913.
38) S. Hengsberger, A. Kulik, and P. Zysset: Bone **30** (2002) 178.
39) S. Hengsberger, J. Enstroem, F. Peyrin, and P. Zysset: J. Biomech. **36** (2003) 1503.
40) I. Eckardt and H. J. Hein: Ann. Biomed. Eng. **29** (2001) 1043.
41) C. H. Turner, J. Rho, Y. Takano, T. Y. Tsui, and G. M. Pharr: J. Biomech. **32** (1999) 437.
42) I. Ihara, T. Sawa, and K. Tanaka: Jpn. J. Appl. Phys. **40** (2001) 3442.
43) J. Y. Rho: Ultrasonics **34** (1996) 777.
44) M. Pithioux, P. Lasaygues, and P. Chabrand: J. Biomech. **35** (2002) 961.
45) A. J. Bushby, V. L. Ferguson, and A. Boyde: J. Mater. Res. **19** (2004) 249.